

# Deep reinforcement learning for smart calibration of radio telescopes

Sarod Yatawatta<sup>1</sup><sup>★</sup> and Ian M. Avruch<sup>†</sup>

<sup>1</sup>*ASTRON, Oude Hoogeveensedijk 4, 7991 PD Dwingeloo, The Netherlands*

5 November 2021

## ABSTRACT

Modern radio telescopes produce unprecedented amounts of data, which are passed through many processing pipelines before the delivery of scientific results. Hyperparameters of these pipelines need to be tuned by hand to produce optimal results. Because many thousands of observations are taken during a lifetime of a telescope and because each observation will have its unique settings, the fine tuning of pipelines is a tedious task. In order to automate this process of hyperparameter selection in data calibration pipelines, we introduce the use of reinforcement learning. We use a reinforcement learning technique called twin delayed deep deterministic policy gradient (TD3) to train an autonomous agent to perform this fine tuning. For the sake of generalization, we consider the pipeline to be a black-box system where only an interpreted state of the pipeline is used by the agent. The autonomous agent trained in this manner is able to determine optimal settings for diverse observations and is therefore able to perform *smart* calibration, minimizing the need for human intervention.

**Key words:** Instrumentation: interferometers; Methods: numerical; Techniques: interferometric

## 1 INTRODUCTION

Data processing pipelines play a crucial role for modern radio telescopes, where the incoming data flow is reduced in size by many orders of magnitude before science-ready data are produced. In order to achieve this, data are passed through many processing steps, for example, to mitigate radio frequency interference (RFI), to remove strong confusing sources and to correct for systematic errors. Calibration is one crucial step in these interferometric processing pipelines, not only to correct for systematic errors in the data, but also to subtract strong outlier sources such that weak RFI mitigation can be carried out. Most modern radio telescopes are general purpose instruments because they serve diverse science cases. Therefore, depending on the observational parameters such as the direction in the sky, observing frequency, observing time (day or night) etc., the processing pipelines need to be adjusted to realize the potential quality of the data.

The best parameter settings for each pipeline are mostly determined by experienced astronomers. This requirement for hand tuning is problematic for radio telescopes that stream data uninterruptedly. In this paper, we propose the use of autonomous agents to replace the human aspect in fine-tuning pipeline settings. We focus on calibration pipelines, in particular, distributed calibration pipelines where data at multiple frequencies are calibrated together, in a distributed computer (Yatawatta 2015; Brossard et al. 2016; Yatawatta et al. 2018; Ollier et al. 2018; Yatawatta 2020). In this setting, the smoothness of systematic errors across frequency is exploited to get a better quality solution, as shown by results with real and simulated data (Patil et al. 2017; Mertens et al. 2020; Mevius et al. 2021).

The key hyperparameter that needs fine-tuning in a distributed calibration setting is the regularization factor for the smoothness of

solutions across frequency. It is possible to select the regularization analytically (Yatawatta 2016), however, extending this to calibration along multiple directions (where each direction will have a unique regularization factor) is not optimal. In this paper, we train an autonomous agent to predict the regularization factors for a distributed, multi-directional calibration pipeline. The calibration pipeline will perform calibration with a cadence of a few seconds to a few minutes of data. Therefore, for an observation of long duration the calibration pipeline needs to be run many times. At the beginning of every observation the autonomous agent will recommend the regularization factors to be used in the pipeline based on the pipeline *state* and will update the factors at the required cadence.

We train the autonomous agent using reinforcement learning (RL) (Sutton & Barto 2018). Reinforcement learning is a branch of machine learning where an agent is trained by repeated interactions with its environment, with proper rewards (or penalties) awarded whenever a correct (or incorrect) decision (or action) is made. In our case, the environment or the observations made by the agent are i) the input data to the pipeline ii) the input sky model to the pipeline used in calibration, and, iii) the output solutions iv) the output residual data from the pipeline. However, we do not feed data directly to the agent, instead, only an interpretation of the pipeline state is fed to the agent. Because the calibration is done on data at a small time duration, the amount of data used to determine this state is also small (compared with the full observation). The determination of the reward is done considering two factors. First, the calibration should perform accurately such that the variance of the residual data should be lower than the input data (scaled by the correction applied during calibration). Secondly, we should not overfit the data, which will suppress signals of scientific interest in the residual. In order to measure the overfitting, we use the influence function (Cook & Weisberg 1982; Koh & Liang 2017) which we can calculate in closed form (Yatawatta 2019). Therefore, the reward is determined by considering both the noise reduction as well as the influence function of calibration. To

<sup>★</sup> E-mail: yatawatta@astron.nl

<sup>†</sup> E-mail: ian.professional@avruch.net

summarize, we consider both the bias and the variance (Geman et al. 1992) introduced by the pipeline for the determination of the state as well as the reward. The agent will perform an action, that is to recommend the optimal regularization factors to use in the calibration pipeline.

The advent of deep neural networks (deep learning) (LeCun et al. 2015) combined with better training algorithms have enabled RL agents to perform superhuman tasks. Early RL breakthroughs were made in discrete action spaces such as in computer games (Mnih et al. 2015). The regularization factors used in calibration are in a continuous action space, and therefore, in this paper we use RL techniques suitable for continuous action spaces, namely, deep deterministic policy gradient (DDPG) (Lillicrap et al. 2015) and its improvement, TD3 (Fujimoto et al. 2018). In this paper, we only consider calibration pipelines that perform distributed, direction dependent calibration, but the same RL technique can be used in other data processing pipelines in radio astronomy and beyond.

The rest of the paper is organized as follows. In section 2, we describe the distributed, direction dependent calibration pipeline. In section 3, we introduce our RL agent and its environment. In section 4, we provide results based on simulated data to show the efficacy of the trained RL agent. Finally, we draw our conclusions in section 5.

*Notation:* Lower case bold letters refer to column vectors (e.g.  $\mathbf{y}$ ). Upper case bold letters refer to matrices (e.g.  $\mathbf{C}$ ). Unless otherwise stated, all parameters are complex numbers. The set of complex numbers is given as  $\mathbb{C}$  and the set of real numbers as  $\mathbb{R}$ . The matrix inverse, pseudo-inverse, transpose, Hermitian transpose, and conjugation are referred to as  $(\cdot)^{-1}$ ,  $(\cdot)^\dagger$ ,  $(\cdot)^T$ ,  $(\cdot)^H$ ,  $(\cdot)^\star$ , respectively. The matrix Kronecker product is given by  $\otimes$ . The vectorized representation of a matrix is given by  $\text{vec}(\cdot)$ . The identity matrix of size  $N$  is given by  $\mathbf{I}_N$ . All logarithms are to the base  $e$ , unless stated otherwise. The Frobenius norm is given by  $\|\cdot\|$  and the L1 norm is given by  $\|\cdot\|_1$ .

## 2 DISTRIBUTED DIRECTION DEPENDENT CALIBRATION PIPELINE

In this section, we give a brief overview of the distributed, direction dependent calibration pipeline that is used by the RL agent for hyperparameter tuning. We refer the reader to Yatawatta (2015) for an in-depth overview of its operation.

The signal received by an interferometer is given by (Hamaker et al. 1996)

$$\mathbf{V}_{pqf} = \sum_{k=1}^K \mathbf{J}_{kp} \mathbf{C}_{kpqf} \mathbf{J}_{kq}^H + \mathbf{N}_{pqf} \quad (1)$$

where we have signals from  $K$  discrete sources in the sky being received. All items in (1), i.e.,  $\mathbf{V}_{pqf}$ ,  $\mathbf{C}_{kpqf}$ ,  $\mathbf{J}_{kp}$ ,  $\mathbf{J}_{kq}$ ,  $\mathbf{N}_{pqf} \in \mathbb{C}^{2 \times 2}$  are implicitly time varying and subscripts  $p, q$  correspond to stations  $p$  and  $q$ ,  $f$  correspond to the receiving frequency, and  $k$  correspond to the source index. The coherency of the  $k$ -th source at baseline  $p-q$  is given by  $\mathbf{C}_{kpqf}$  and for a known source, this can pre-computed (Thompson et al. 2001). The noise  $\mathbf{N}_{pqf}$  consists of the actual thermal noise as well as signals from sources in the sky that are not part of the model. The systematic errors due to the propagation path (ionosphere), receiver beam, and receiver electronics are represented by  $\mathbf{J}_{kp}$  and  $\mathbf{J}_{kq}$ . For each time and frequency, with  $N$  stations, we have  $N(N-1)/2$  pairs of  $p-q$ .

Calibration is the estimation of  $\mathbf{J}_{kp}$  for all  $p$  and  $f$ , using data within a small time interval (say  $T$ ), within which it is assumed that  $\mathbf{J}_{kp}$  remains constant. An important distinction is that we only calibrate along  $K$  directions, but in real observations, there is always

signals from faint sources (including the Galaxy) that are not being modeled. We are not presenting a method of calibration in this paper, and therefore the actual method of calibration is not relevant. However, for the sake of simplicity, we follow a straightforward description. What we intend to achieve is to relate the hyperparameters used in the pipeline to the performance of calibration. Therefore, we represent  $\mathbf{J}_{kp}$  as 8 real parameters (for frequency  $f$  and direction  $k$ ), and we have  $8 \times N \times K$  real parameters in total for frequency  $f$ , per direction, namely  $\theta_{kf}$ .

We represent (1) in vector form as

$$\mathbf{v}_{pqf} = \sum_{k=1}^K \mathbf{s}_{kpqf}(\theta_{kf}) + \mathbf{n}_{pqf} \quad (2)$$

where  $\mathbf{s}_{kpqf}(\theta_{kf}) = (\mathbf{J}_{kq}^\star \otimes \mathbf{J}_{kp}) \text{vec}(\mathbf{C}_{kpqf})$ ,  $\mathbf{v}_{pqf} = \text{vec}(\mathbf{V}_{pqf})$ , and  $\mathbf{n}_{pqf} = \text{vec}(\mathbf{N}_{pqf})$ .

We stack up the data and model vectors of (2) for the  $T$  time slots within which a single solution is obtained as

$$\begin{aligned} \mathbf{x}_f &= [\text{real}(\mathbf{v}_{12}^T), \text{imag}(\mathbf{v}_{12}^T), \text{real}(\mathbf{v}_{13}^T), \dots]^T \\ \mathbf{s}_{kf}(\theta_{kf}) &= [\text{real}(\mathbf{s}_{k12f}(\theta)^T), \text{imag}(\mathbf{s}_{k12f}(\theta)^T), \text{real}(\mathbf{s}_{k13f}(\theta)^T), \dots]^T \end{aligned} \quad (3)$$

which are vectors of size  $8 \times N(N-1)/2 \times T$  and we have

$$\mathbf{x}_f = \sum_{k=1}^K \mathbf{s}_{kf}(\theta_{kf}) + \mathbf{n}_f = \mathbf{s}_f(\theta_f) + \mathbf{n}_f \quad (4)$$

as our final measurement equation  $\theta_{kf} \in \mathbb{R}^{8N}$ ,  $\theta_f \in \mathbb{R}^{8KN}$ .

In order to estimate  $\theta_{kf}$  from (4), we define a loss function

$$g_{kf}(\theta_{kf}) = \text{loss}(\mathbf{x}_f, \theta_{kf}) \quad (5)$$

depending on the noise model, for example, mean squared error loss,  $\|\mathbf{x}_f - \mathbf{s}_f(\theta_f)\|^2$ . We calibrate data at many frequencies and we exploit the smoothness of  $\theta_{kf}$  with  $f$  and in order to make the solutions smooth, we introduce the constraint

$$\theta_{kf} = \mathbf{Z}_k \mathbf{b}_f \quad (6)$$

where  $\mathbf{b}_f \in \mathbb{R}^P$  is a polynomial basis ( $P$  terms) evaluated at  $f$  and  $\mathbf{Z}_k \in \mathbb{R}^{8N \times P}$  is the global variable ensuring smoothness across frequency.

With the use of Lagrange multipliers  $\mathbf{y}_{kf} \in \mathbb{R}^{8N}$ , we write the augmented Lagrangian as

$$l(\theta_{kf}, \mathbf{y}_{kf}, \mathbf{Z}_k : \forall k, f) = \quad (7)$$

$$\sum_{kf} g_{kf}(\theta_{kf}) + \rho_k \mathbf{y}_{kf}^T (\theta_{kf} - \mathbf{Z}_k \mathbf{b}_f) + \frac{\rho_k^2}{2} \|\theta_{kf} - \mathbf{Z}_k \mathbf{b}_f\|^2$$

which we minimize to find a smooth solution.

The hyperparameters in (7) are the regularization factors  $\rho_k \in \mathbb{R}^+$ , we have one regularization factor per each direction  $k$ . Therefore, we need to select  $K$  positive, real valued hyperparameters to get the optimal solution to (7). We can consider the  $K$  directional calibration as  $K$  separate subproblems and find analytical solutions to optimal  $\rho_k$  as done in Yatawatta (2016), however this is not optimal. The alternative is to use handcrafted methods such as grid search, but because each observation is unique, performing this for every observation is not feasible. In the next section, we will present the use of RL to automatically find the best values for  $\rho_k$ .

The RL agent interacts with the pipeline (the pipeline is solving (7)) to recommend the best values for  $\rho_k$ . In order to do this, the RL

agent needs to have some information about the environment (i.e., the performance of the pipeline). In Fig. 2, we show the interactions between the agent and the pipeline. After each calibration, we calculate the residual as

$$\mathbf{R}_{pqf} = \mathbf{V}_{pqf} - \sum_{k=1}^K \hat{\mathbf{J}}_{kp f} \mathbf{C}_{kp q f} \hat{\mathbf{J}}_{kq f}^H \quad (8)$$

where  $\hat{\mathbf{J}}_{kp f} \forall k, p, f$  are calculated using the solutions obtained for  $\theta_{kf}$ .

We can rewrite (4) in a simplified form (dropping the subscripts  $k, f$ ) as

$$\mathbf{x} = \mathbf{s}(\theta) + \mathbf{n} \quad (9)$$

where  $\mathbf{x} (\in \mathbb{R}^D)$  is the data,  $\mathbf{s}(\theta)$  is our model and  $\mathbf{n}$  is the noise. We find a solution to  $\theta$  by minimizing a loss  $g(\theta)$ , say  $\hat{\theta}$ . Thence, we calculate the residual as

$$\mathbf{y} = \mathbf{x} - \mathbf{s}(\hat{\theta}). \quad (10)$$

We have shown (Yatawatta 2019) that the probability density functions of  $\mathbf{x}$  and  $\mathbf{y}$ , i.e.,  $p_X(\mathbf{x})$ ,  $p_Y(\mathbf{y})$  are related as

$$p_X(\mathbf{x}) = |\mathcal{J}| p_Y(\mathbf{y}) \quad (11)$$

where  $|\mathcal{J}|$  is the Jacobian determinant of the mapping from  $\mathbf{x}$  to  $\mathbf{y}$ . Using (10), we can show that

$$|\mathcal{J}| = \exp \left( \sum_{i=1}^D \log(1 + \lambda_i(\mathcal{A})) \right) \quad (12)$$

where

$$\mathcal{A} = \frac{\partial \mathbf{s}(\theta)}{\partial \theta^T} \left( \frac{\partial^2 g(\theta)}{\partial \theta \partial \theta^T} \right)^{-1} \frac{\partial^2 g(\theta)}{\partial \theta \partial \mathbf{x}^T} \quad (13)$$

evaluated at  $\theta = \hat{\theta}$ . Ideally, we should have  $|\mathcal{J}| = 1$  and therefore all eigenvalues of  $\mathcal{A}$ ,  $\lambda_i(\mathcal{A}) = 0$ . But in practice, due to model error and degeneracies in the model, we have some non-zero values for  $\lambda_i(\mathcal{A})$ .

Using (13), we can calculate  $E\{\frac{\partial \mathbf{R}_{pqf}}{\partial x_{p'q'l f}}\}$  for the residual  $\mathbf{R}_{pqf}$  in (8), where the expectation  $E\{\cdot\}$  is taken over  $p', q'$  (excluding the tuple  $p, q$ ) and  $l \in [1, 8]$ . We call the image made in the usual radio astronomical image synthesis manner, replacing the residual  $\mathbf{R}_{pqf}$  with  $E\{\frac{\partial \mathbf{R}_{pqf}}{\partial x_{p'q'l f}}\}$ , as the *influence map*, which we denote by  $\mathcal{I}(\theta)$ .

In Fig. 1, we show a montage of  $\mathcal{I}(\theta)$  generated in our simulations (see section 4). All the images shown in Fig. 1 are made using the same  $uv$  coverage, and the images are not deconvolved with the PSF. Therefore, the only reason for the differences in these images are the sky models (the true sky and the sky model used in calibration) and the performance of the calibration pipeline itself. Therefore, influence maps serve a useful purpose in diagnosing the performance of calibration (Yatawatta 2019).

We relate the influence map to the bias and variance of calibration residual as follows. The bias is primarily caused by the errors in the sky model (difference between the true sky and the sky model used in calibration). Therefore, with low regularization, we have high bias, high influence and low variance. With high regularization, we have low bias, low influence and high variance. An example of this behavior is shown in Fig. 4. Note that we consider the bias and variance of the residual data, and not the bias and variance of the solutions of calibration. If we consider the solutions, with low regularization we will have low bias and high variance (overfitting compared to the ground truth) and with high regularization, we will

have high bias and low variance (underfitting). The fine tuning of  $\rho_k$  will give us the optimal tradeoff between bias and the variance of the residual data, and we achieve this by RL as described in section 3.

### 3 REINFORCEMENT LEARNING

In this section, we describe the basic concepts of reinforcement learning, especially tailored to our problem and thereafter we go into specific details about our RL agent. A RL agent interacts with its environment via some observations and performs an action depending on these observations and the current state of the agent. The objective of the agent is to maximize its reward depending on the action it performs. As shown in Fig. 2, our agent interacts with our calibration pipeline, which is the environment. We describe these interactions as follows:

- At an instance indexed by  $t$ , the input to the agent is given by state  $s_t$ . This is a summary of the observation that we deem sufficient for the agent to evaluate its action. In our case, we give the sky model used in calibration as part of  $s_t$ . In addition, we create an influence map (an image), that summarizes the performance of calibration as part of  $s_t$ . Note that we do not feed the data or the metadata (such as the  $uv$  coverage) into the agent.
- Depending on  $s_t$  and its internal parameter values, the agent performs an action  $a_t$ . In our case, the action is specification of the regularization factors  $\rho_k$  ( $K$  values) which is fed back to the pipeline.
- We determine the reward  $r_t$  (a real valued scalar) to the agent using two criteria. First, we compare the noise of the input data  $\sigma_0$  and the output residual  $\sigma_1$  of the pipeline (by making images of the field being observed) and find the ratio  $\frac{\sigma_0}{\sigma_1}$ . We get a higher reward if the noise is reduced. Second, we look at the influence map and find its standard deviation, which we add to the reward. If we have high influence (high bias), we will get a smaller reward. With both these components constituting the reward, we aim to minimize both the bias and the variance of the pipeline.

Note that unlike in most RL scenarios, we do not have a terminal state (such as in a computer game where a player wins or loses). We terminate when we reach a certain number of iterations of refinement on  $\rho_k$ .

We give an overview of the inner workings of our RL agent, and for a more thorough overview, we refer the reader to (Silver et al. 2014; Lillicrap et al. 2015; Fujimoto et al. 2018). The major components of the agent are:

- Actor: the actor with policy  $\pi(\cdot)$  will produce action  $a$  given the state  $s$ ,  $\pi(s) \rightarrow a$ .
- Critic: given the state  $s$  and action  $a$ , the critic will evaluate the expected return  $q$  (a scalar),  $Q(s, a) \rightarrow q$ . The mapping  $Q(\cdot, \cdot)$  is also called as the state-action value function.

Note that neither the actor nor the critic are dependent on past states, but only the current state and a measure of the state's favorability for future rewards, which is a characteristic of a Markov decision process (Sutton & Barto 2018). Looking into the future, the expected cumulative reward can be written as the Bellman equation

$$Q^*(s, a) = r + \gamma \max_{a'=\pi(s')} Q(s', a') \quad (14)$$

where  $s', a'$  is the (optimal) state action pair for the next step and  $\gamma \approx 1$  is the discount factor for future uncertainty.

We model both the actor and the critic as deep neural networks, with trainable parameters  $\phi$  for the actor and  $\xi$  for the critic. We train

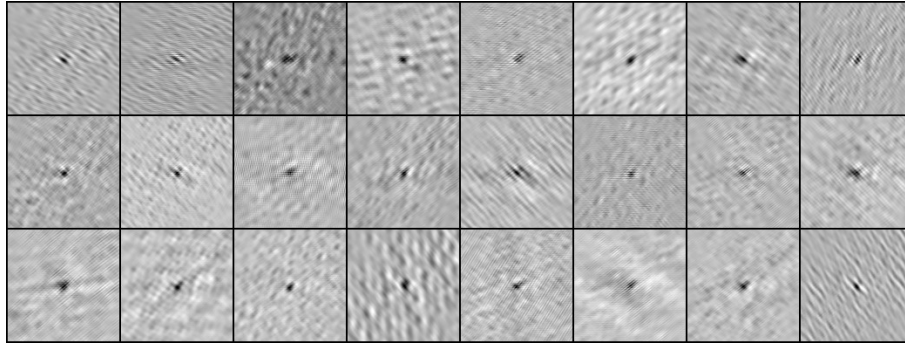


**Figure 1.** A montage of influence maps  $128 \times 128$  pixels each, centered at the phase centre, generated with various calibration settings and sky models. All these maps are created using the same  $uv$  coverage. The values in each influence map are normalized to the range  $[0, 1]$ .

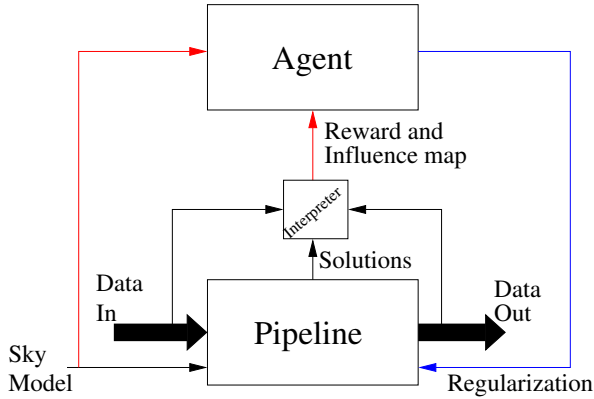


**Figure 2.** The interactions between the RL agent and its environment, i.e., the pipeline.

the actor and the critic as follows. Given the current state  $s$ , the actor tries to maximize  $J(\phi) = Q(s, a)|_{a=\pi(s)}$  by choice of action. We perform gradient ascent on  $J(\phi)$ , with the gradient (using the chain rule) given as

$$\nabla_{\phi} J(\phi) = \nabla_a Q(s, a)|_{a=\pi(s)} \times \nabla_{\phi} \pi(s). \quad (15)$$

The critic is trained by minimizing the error between the current state-action value  $Q(s, a)$  and the expected cumulative reward under optimal settings (14)

$$J(\xi) = \|Q_{\xi}(s, a) - (r + \gamma \max_{a'=\pi(s')} Q(s', a'))\|^2. \quad (16)$$

In practice, RL is prone to instability and divergence, and therefore we follow van Hasselt et al. (2015); Lillicrap et al. (2015); Fujimoto et al. (2018) with the following refinements:

- Instead of having one critic, we have two online ( $Q_1(s, a)$  and  $Q_2(s, a)$ ) and two target ( $Q_1(s', a')$  and  $Q_2(s', a')$ ) critics and select the lower evaluation out of the two to evaluate (14).
- Rather than having just one actor, we also have a target actor network. When evaluating (14), we use the target network to evaluate  $\max_{a'=\pi(s')} Q(s', a')$ .
- The parameters of the target networks are updated by a weighted average between the online and target parameters, and for the target actor, the update is only performed at delayed intervals.

- We use random actions at the start of learning for exploration, which is called the warmup period.
- We keep a buffer to store past actions, current states, next states and rewards that we re-use in mini-batch mode sampling during training (this is called the replay buffer).

See Algorithm I (Fujimoto et al. 2018) for a detailed description of the TD3 algorithm.

## 4 SIMULATIONS

Simulations are required to train the RL agent. In this section, we present the details of our simulations and show that the agent is able to learn, in other words, with more training, the reward obtained by the agent increases.

Before we proceed to describing the agent used in radio interferometric calibration pipelines, we consider a much simpler problem. This is to test and demonstrate the efficacy of our reinforcement learning algorithm (TD3), which has already been proven to be superior in other environments. However, we did not find an analogue to hyperparameter tuning. Elastic net regression (Zou & Hastie 2005) observes  $\mathbf{x} \in \mathbb{R}^D$  given the design matrix  $\mathbf{A} \in \mathbb{R}^{D \times D}$  and estimates the parameters  $\boldsymbol{\theta} \in \mathbb{R}^D$  of the linear model  $\mathbf{x} = \mathbf{A}\boldsymbol{\theta}$ . The estimation is performed under regularization as

$$\hat{\boldsymbol{\theta}} = \arg \min_{\boldsymbol{\theta}} \left( \|\mathbf{x} - \mathbf{A}\boldsymbol{\theta}\|^2 + \rho_2 \|\boldsymbol{\theta}\|^2 + \rho_1 \|\boldsymbol{\theta}\|_1 \right) \quad (17)$$

where we have hyperparameters  $\rho_1$  and  $\rho_2$ . We can easily relate (17) to (7), which is our original problem.

Representing (17) as in (9) and using (13), for the elastic net problem, we have

$$\mathcal{A} = \mathbf{A} \frac{1}{2} \left( \mathbf{A}^T \mathbf{A} + \rho_2 \mathbf{I} \right)^{-1} \left( -2\mathbf{A}^T \right) \quad (18)$$

which can be used to calculate the influence function. The RL agent for the elastic net problem hyperparameter selection interacts with its environment as follows:

- State: design matrix  $\mathbf{A}$  and eigenvalues  $(1 + \lambda(\mathcal{A}))$ .
- Action: regularization factors  $\rho_1, \rho_2$ .
- Reward:  $\frac{\|\mathbf{x}\|}{\|\mathbf{x} - \mathbf{A}\boldsymbol{\theta}\|} + \frac{\min(1 + \lambda(\mathcal{A}))}{\max(1 + \lambda(\mathcal{A}))}$ .

Note that the reward considers both the (inverse) residual error as well as the bias (ratio of eigenvalues of the influence matrix). In this manner, we can achieve a balance between the bias and the variance of the residual.



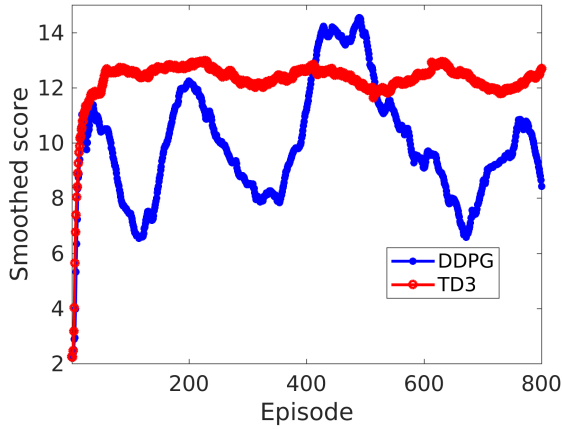


**Figure 3.** The smoothed score variation with episode for the agent selecting hyperparameters in elastic net regression.

We consider  $D = 20$  and the agent is implemented in Pytorch (Paszke et al. 2017), within an *openai.gym* compatible environment<sup>1</sup>. The critic uses 2 linear layers each for the state and for the action, finally combined in one linear layer to produce a scalar output. The actor uses three linear layers to produce the 2 dimensional output. We use exponential linear unit activation (Clevert et al. 2015) except in the last layer of the actor, where we use hyperbolic tangent activation (which is scaled to the valid range afterwards). We use batch normalization (Ioffe & Szegedy 2015) between all layers except the last. We use the LBFGS algorithm Yatawatta et al. (2019) to solve (17) and the Adam optimizer Kingma & Ba (2014) is used to train the agent.

In each episode, we create  $\mathbf{A}$  by filling its entries with unit variance, zero mean Gaussian random values. The ground truth value of the parameters,  $\theta_0$  is generated with the number of non-zero entries randomly generated in the range  $[3, D]$  and these non-zero entries are filled with unit variance, zero mean Gaussian entries. In order to get  $\mathbf{x}$ , we add unit variance, zero mean Gaussian noise to  $\mathbf{A}\theta_0$  with a signal to noise ratio of 0.1.

For each episode, we limit the number of iterations to 30 (chosen arbitrarily). In each iteration, the tuple (state, action, reward, next state) are determined and stored in the replay buffer. After the initial warmup interval (100 iterations), we start the learning process. In Fig. 3, we show the smoothed reward after each episode. We have compared DDPG algorithm with TD3 algorithm. We clearly see the stability of TD3 that justifies using TD3 algorithm to train our calibration pipeline agent.

We give a summary of the calibration pipeline. The data passed through the calibration pipeline have 1 sec integration time and 8 frequencies in the range  $[115, 185]$  MHz. Calibration is performed for every  $T = 10$  time samples (every 10 sec) and 6 such calibrations are performed to interact with the RL agent. In other words, 1 min of data are used by the agent to make a recommendation on the regularization parameters. In practice, the first 1 min of data is used to adjust the hyperparameters of the pipeline, and thereafter, the pipeline is run unchanged for the full observation (which typically

will last a few hours). We use SAGECal<sup>2</sup> for calibration and excon<sup>3</sup> for imaging.

We simulate data for calibration along  $K = 4$  directions in the sky, with systematic errors  $\mathbf{J}_{kpf}$  in (1) that are smooth both in time and in frequency, but have random initial values. One direction out of  $K$  represents the observed field, and its location is randomly chosen within 1 deg radius from the field centre. The remaining  $K - 1$  directions play the role of outlier sources (for instance sources such as the Sun, Cassiopeia A, Cygnus A) and are randomly located within a 15 deg radius from the field centre. The intensity of the central source is randomly selected within  $[3, 10]$  Jy. The intrinsic intensities of the outlier sources are randomly selected within  $[100, 250]$  Jy. An additional 200 weak sources (point sources and Gaussians) with intensities in  $[0.01, 0.1]$  Jy are randomly positioned across a  $16 \times 16$  square degrees surrounding the field centre. The spectral indices of all sources are also randomly generated. The simulation includes the effect due to the station beam shape. Finally, zero mean, complex circular Gaussian noise is added to the simulated data with a signal to noise ratio of 0.05. Note that the sky model used for calibration only includes the  $K$  sources (not the weak sources) and the  $K - 1$  outlier sources have their intensities reduced by a factor of 100 (apparent value).

The RL agent used in the calibration pipeline interacts with the environment (or the pipeline) as follows:

- State: the sky model used in calibration and the influence map  $\mathcal{I}(\theta)$  generated using 1 min of data.
- Action: regularization factors  $\rho_k$  for  $K$  directions.
- Reward:  $\frac{\sigma_0}{\sigma_1} + \frac{1}{B\sigma(\mathcal{I}(\theta))}$ , where  $\sigma_0$  and  $\sigma_1$  are the image noise standard deviations of the input data and output residual, respectively.  $B = 8TN(N-1)/2$  is the total number of data points used to calculate  $\mathcal{I}(\theta)$  and  $\sigma(\mathcal{I}(\theta))$  is the standard deviation of the influence map.

In Fig. 4, we show the residual image standard deviation, influence map standard deviation and the calculated reward. The  $x$ -axis corresponds to the regularization parameters  $\rho_k$ , scaled up and down by various factors (starting from the regularization that gives the highest reward). For low regularization values, we see more or less constant residual image noise, however, we clearly see a high level of influence. This high influence on the left hand side of Fig. 4 implies high bias (due to the unmodeled sources in the sky) and as a consequence, we should expect high level of weak signal suppression. On the other hand, on the right hand side of Fig. 4, for high regularization, we see increased residual image noise, meaning poor calibration. We compose our reward to reach a balance between the bias and variance of the residual.

The RL agent and environment are quite similar to the ones used in elastic net regression. The critic uses 3 convolutional layers to process the influence map, and two linear layers to process the action and the sky model. These two are combined at the final linear layer. The actor also uses 3 convolutional layers to process the influence map and two linear layers for the sky model. Once again, they are combined at the final linear layer. The first three layers of both the actor and critic use batch normalization. The activation functions are exponential linear units except at the last layer of the actor, where we use hyperbolic tangent activation. The action is scaled to the required range by the environment.

The training of our RL agent is done as follows. In each episode, we generate a random sky model and data as described previously.

<sup>1</sup> <https://gym.openai.com/>

<sup>2</sup> <http://sagecal.sourceforge.net/>

<sup>3</sup> <https://sourceforge.net/projects/exconimager/>

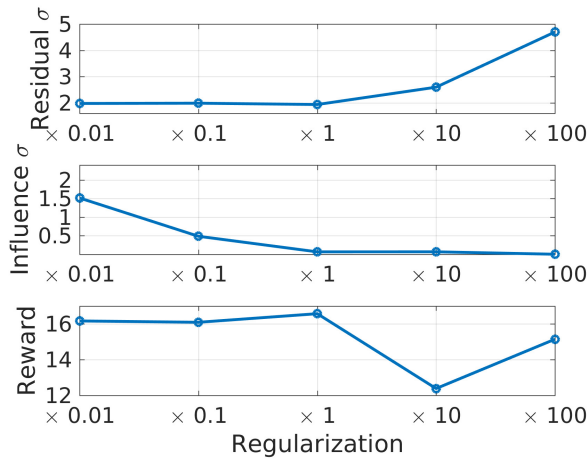


**Figure 4.** The residual noise, the influence map noise and the reward for various values of regularization. The regularization factors are scaled up and down from the optimal values ( $\times 1$ ).

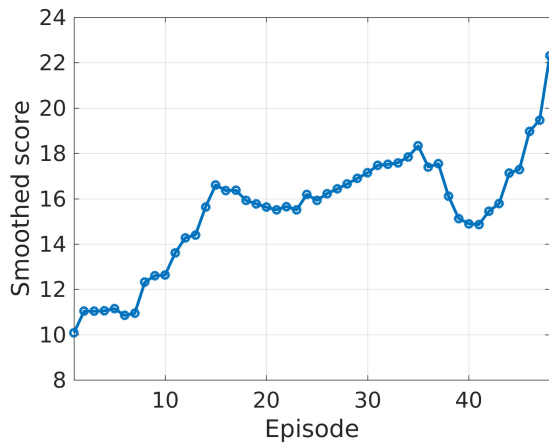


**Figure 5.** The smoothed score variation with episode for the agent in the calibration pipeline.

The pipeline is run with initial regularization factors determined analytically (Yatawatta 2016). The state information generated by the pipeline is fed into the RL agent to retrieve updated regularization factors. The pipeline is run again and we repeat the cycle. We limit the number of such iterations per each episode to 10 (arbitrary number). At the final iteration, we record the reward (or the score) to measure the progress of the agent. The smoothed score over a number of such episodes is shown in Fig. 5. We see a positive trend in the score in Fig. 5, indicating that the agent is able to learn and improve its recommendations for the regularization factors to use. We also see a small dip around the 35-th episode, where we switched from learning to warmup mode (exploration instead of exploitation), where instead of choosing the action based on the output of the actor, we switched to random actions (because we re-started the training at episode 32).

Once we have a fully trained agent, we only have to run one iteration to get a recommendation from the agent. Note that we have used only 1 min of data for this and afterwards, we can keep the pipeline running with the same hyperparameters for a much longer

time (ideally for the full observation). This aspect needs more work with real data, which we intend to pursue as future work. In addition, we can develop similar agents for other data processing steps in radio astronomy, including RFI mitigation and image synthesis. Extending beyond radio astronomy, similar techniques can be applied in other data processing pipelines in general machine learning problems.

## 5 CONCLUSIONS

We have introduced the use of reinforcement learning in hyperparameter tuning of radio astronomical calibration pipelines. By using both the input-output noise reduction as well as the influence to determine the reward offered to the RL agent, we can reach a balance between the bias and the variance introduced by the pipeline. As illustrated by the elastic-net regression example, we can also apply the same technique to many other data processing steps, not only in radio astronomy but also in other applications.

## DATA AVAILABILITY

Ready to use software based on this work and test data are already available online<sup>4</sup>.

## REFERENCES

- Brossard M., El Korso M. N., Pesavento M., Boyer R., Larzabal P., Wijnholds S. J., 2016, preprint, ([arXiv:1609.02448](https://arxiv.org/abs/1609.02448))
- Clevert D.-A., Unterthiner T., Hochreiter S., 2015, arXiv e-prints,
- Cook R., Weisberg S., 1982, *Residuals and Influence in Regression*. Monographs on statistics and applied probability, Chapman & Hall, <http://books.google.nl/books?id=MVSqAAAAIAAJ>
- Fujimoto S., van Hoof H., Meger D., 2018, arXiv e-prints, p. [arXiv:1802.09477](https://arxiv.org/abs/1802.09477)
- Geman S., Bienenstock E., Doursat R., 1992, *Neural Computation*, 4, 1
- Hamaker J. P., Bregman J. D., Sault R. J., 1996, *Astronomy and Astrophysics Supp.*, 117, 96
- Ioffe S., Szegedy C., 2015, arXiv e-prints, p. [arXiv:1502.03167](https://arxiv.org/abs/1502.03167)
- Kingma D. P., Ba J., 2014, preprint, ([arXiv:1412.6980](https://arxiv.org/abs/1412.6980))
- Koh P. W., Liang P., 2017, in Precup D., Teh Y. W., eds, *Proceedings of Machine Learning Research* Vol. 70, Proceedings of the 34th International Conference on Machine Learning. PMLR, International Convention Centre, Sydney, Australia, pp 1885–1894, <http://proceedings.mlr.press/v70/koh17a.html>
- LeCun Y., Bengio Y., Hinton G., 2015, *Nature*, 521, 436 EP
- Lillicrap T. P., Hunt J. J., Pritzel A., Heess N., Erez T., Tassa Y., Silver D., Wierstra D., 2015, arXiv e-prints, p. [arXiv:1509.02971](https://arxiv.org/abs/1509.02971)
- Mertens F., et al., 2020, *Monthly Notices of the Royal Astronomical Society*, 493, 1662
- Mevius M., et al., 2021, pre-print
- Mnih V., et al., 2015, *Nature*, 518, 529
- Ollier V., Korso M. N. E., Ferrari A., Boyer R., Larzabal P., 2018, *Signal Processing*, 153, 348
- Paszke A., et al., 2017, in *NIPS-W*.
- Patil A. H., et al., 2017, *ApJ*, 838, 65
- Silver D., Lever G., Heess N., Degris T., Wierstra D., Riedmiller M., 2014, in *Proceedings of the 31st International Conference on International Conference on Machine Learning - Volume 32*. ICML 2014. JMLR.org, pp 387–395
- Sutton R. S., Barto A. G., 2018, *Reinforcement Learning: An Introduction*. A Bradford Book, Cambridge, MA, USA

<sup>4</sup> <https://github.com/SarodYatawatta/smart-calibration>

- Thompson A., Moran J., Swenson G., 2001, *Interferometry and synthesis in radio astronomy* (3rd ed.). Wiley Interscience, New York
- Yatawatta S., 2015, *MNRAS*, 449, 4506
- Yatawatta S., 2016, in 24th European Signal Processing Conference (EU-SIPCO), 2016.
- Yatawatta S., 2019, *Monthly Notices of the Royal Astronomical Society*, 486, 5646
- Yatawatta S., 2020, *Monthly Notices of the Royal Astronomical Society*, 493, 6071
- Yatawatta S., Diblen F., Spreeuw H., Koopmans L. V. E., 2018, *MNRAS*, 475, 708
- Yatawatta S., De Clercq L., Spreeuw H., Diblen F., 2019, in 2019 IEEE Data Science Workshop (DSW). pp 208–212, doi:10.1109/DSW.2019.8755567
- Zou H., Hastie T., 2005, *Journal of the Royal Statistical Society: Series B (Statistical Methodology)*, 67, 301
- van Hasselt H., Guez A., Silver D., 2015, arXiv e-prints, p. arXiv:1509.06461

This paper has been typeset from a  $\text{\TeX}/\text{\LaTeX}$  file prepared by the author.